2.2 MICROSTRUCTURAL AND MECHANICAL BEHAVIOR OF AS-FABRICATED AND ANNEALED 14YWT NFA-1 ALLOY —

M.E. Alam, S. Pal, D. Gragg, G. R. Odette (UCSB), D. T. Hoelzer (ORNL) and S. A. Maloy (LANL)

OBJECTIVE

The objective of this study is to perform statistical analysis of grains, precipitates and microcracks of as-fabricated 14YWT FCRD NFA-1 material, and to explore the effects of annealing on the microstructural and mechanical properties.

SUMMARY

FCRD NFA-1 is a new 14YWT nanostructured ferritic alloy (NFA) processed to form a 12.5 mm thick plate. Ultrafine, nearly equiaxed grains dominate the plate's face (LT), while the front (LS) and side (TS) views contain pancake-shaped, trimodal grains with very large aspect ratios, along with a population of embedded microcracks that are readily visible in profile. Low temperatures tensile tests on the longitudinal (L) direction show a delamination driven ductile fracture, even at liquid nitrogen temperature, with strengths up to 1563 MPa. In contrast, the room temperature tensile specimen loaded in the short thickness (S) direction fails prematurely in its elastic regime, with a flat, faceted fracture surface. Annealing at 1300°C for 1 and 5 hrs helps to alter the grains towards equiaxed in all plane views and heals the microcracks, which results in much improved room temperature tensile ductility. However, microhardness, tensile strength and fracture toughness have been compromised, and the fracture mechanism has also been changed from delamination driven to microvoid coalescence dimple fracture.

PROGRESS AND STATUS

Materials and Methods

The nanostructured ferritic alloys (NFAs) are a promising candidate alloy class for the advanced nuclear fission and future fusion reactor applications, since they have high tensile, fatigue and creep strengths over a wide range of temperature, as well as unique irradiation tolerance and outstanding thermal stability up to 1000°C. These attributes derive from the presence of submicron size grains, high dislocation densities and especially an ultrahigh population of nanometer size Y-Ti-O rich multifunctional nano-oxides (NOs) [1]. NFA-1 was developed in collaboration between UCSB, ORNL and LANL to explore including Y in the Fe-14Cr-3W-0.4Ti-0.2Y melt prior to gas atomization by ATI Powder Metals (Pittsburgh, PA). However, the Y was phase separated after atomization. Thus, a low interstitial alloy powder (15 kg) variant was ball milled for 40 hours with FeO (52.5 g) to increase the O content and to mechanically alloy the Y into solution. The milling was carried out by Zoz GmbH (Wenden, Germany) using a CM100b attritor mill with a ball to-powder mass ratio of 10:1 and ball size of 5 mm. The milled powders were then consolidated at ORNL by hot extrusion at 850°C. The extruded bar was annealed for 1 hour and then hot cross-rolled to a ≈ 50% thickness reduction, both at 1000°C, to produce a ≈ 12.5 mm thick plate [2]. The basic microstructural and mechanical properties of the as-fabricated plate have been reported elsewhere [3-4]. However, due to the anisotropic nature of the plate along with through-thickness grain variation, the measured grain size of three different planes (face: LT, front: LS and side: TS, see Figure 1) were found inconsistent since the specimens were selected randomly. Therefore, in this present study, a 5mm 5mmx5mm cube has been EDM cut from the middle of the plate thickness and grain size of all three plane views was characterized. In detail crack statistics as well as processed induced impurities were also analyzed. Low temperature tensile tests were performed. Later, as-fabricated specimens from the plate were wrapped in a molybdenum getter foil and annealed in vacuum at 1300°C for 1 and 5 hrs. Microstructural and mechanical characterizations were also performed on the annealed specimens.

Metallurgically ground (up to 1500 grit sand paper) and polished (up to 20 nm colloidal silica) as-fabricated and annealed specimens were observed in scanning electron microscope (SEM, FEI x30) equipped with energy dispersive spectroscopy (EDS) to characterize the pre-test surface morphology. Polished samples were then etched with Kroll's reagent (92% distilled water, 6% nitric acid and 2%

hydrofluoric acid) prior to imaging of grains using SEM and dual beam Scanning Electron Microscope/Focused Ion Beam (SEM/FIB, FEI Helios 600). Longest (l) and shortest (s) dimensions of ~ 500 individual grains from each planes were tabulated from the micrographs using 'ImageJ64' software. The effective grain diameter was taken as d = (l+s)/2 and the aspect ratio as r = l/s. Coarser precipitates were identified using both the SEM and transmission electron microscopy (TEM), equipped with EDS. SEM images were used to measure the average precipitate size, inter-precipitate spacing and stringer spacing. Precipitates were found to be arranged in stringers, rather than random. Therefore, the inter-precipitate spacing along the stringer and stringer spacing along the thickness was considered. Microcracks were also characterized in terms of crack width, crack separation distance, crack length and number density of crack per unit area. Relatively low magnification (x1000) SEM images were chosen to characterize the crack length and their number. Vickers microhardness measurements were performed on polished coupon surfaces at a 500g load using LECO M-400A semi-automated hardness tester, based on the average of 10 to 15 indents. Tensile tests were performed on flat dog-bone shaped sub-sized specimens with a gage section length, width, and thickness of 5.0x1.2x0.5 mm^3. The tensile tests were performed for the as-fabricated longitudinal (L) directions as illustrated in Figure 1, from room temperature down to liquid nitrogen temperature, on an 810 MTS servo-hydraulic universal testing machine equipped with a cooling chamber. Controlled liquid nitrogen-air mixture was injected into the cooling chamber to achieve the targeted cryogenic temperature, and held for 30 to 45 minutes before testing. However, both L and short (S) oriented as-fab and annealed tensile specimens were tested at room temperature. The tensile specimens were sanded with 1500 grit to remove surface contamination, minor defects and local residual stresses due to the EDM used to fabricate them. Loading was carried out at a crosshead speed of 0.30 mm/min, or a strain rate of $\approx 10^{-3}$/s. Except for the small size of the specimens, the tensile properties were determined in accordance with ASTM Standard E8M-13. Fracture toughness tests of as-fabricated and annealed specimens were conducted at room temperature on the L-T oriented fatigue pre-cracked single-edged notch three point bend (3PB) bar specimens with nominal dimensions of 16 mm in length, 3.3 mm in width and 1.65 mm in gross thickness and a/W ≈ 0.5. The same 810 MTS servo-hydraulic testing machine was used for this purpose. The toughness (K_{Jc}) was calculated at the maximum load. Fracture surfaces of the broken tensile and toughness specimens were extensively characterized by SEM.

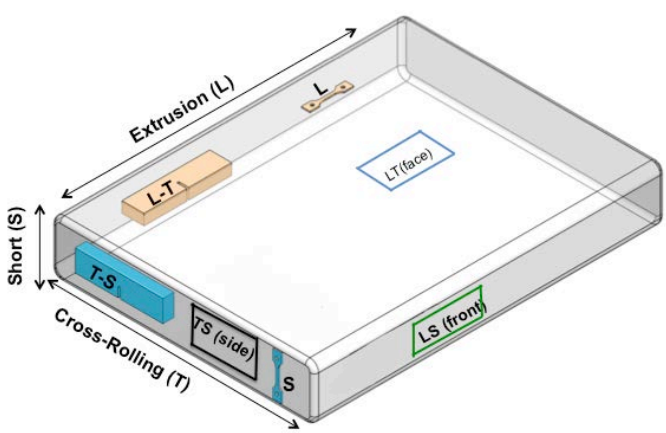

Figure 1. NFA-1 specimen orientations labeled with respect to the extrusion, cross-rolling and plate thickness directions.

Results

Microstructure

The microstructure of the as-fabricated FCRD NFA-1 material has been characterized in terms of: (a) grain morphology, (b) presence and distribution of coarser precipitates, and (c) crack statistics at all three different planes (see Tables 1 to 3 and Figures 1 to 3). Figure 2a and Figure 2b show the low magnification SEM, and high magnification SEM/FIB images of the as-fabricated and pre-test NFA-1 at different planes, respectively. Plate's face (LT) reveals crack or pore free surface. High magnification SEM/FIB images also characterize nearly uniform, equiaxed and ultrafine grain morphology of the corresponding plane (see Table 1). In contrast, the front (LS), and side (TS) views reveal a number of microcracks embedded on planes normal to the plate thickness direction. The corresponding plane's grains are elongated and pancake-shaped that oriented parallel to the extrusion (LS) or cross-rolling (TS) direction with a tri-modal grain size distribution (many are <1 µm, some are 1-10 µm and few are >10 µm, see Figure 3a). Through thickness grain size variation has also been observed. Relatively smaller grains are found near the top and bottom of the plate's thickness while the larger grains at the middle.

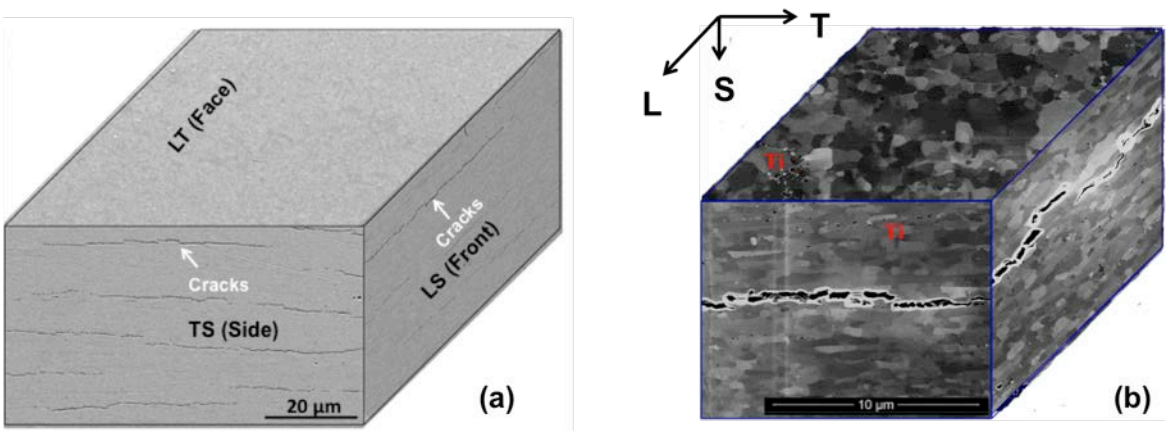

Figure 2. Different plane views of the as-fabricated NFA-1 plate captured by: (a) SEM at low magnification, and (b) SEM/FIB at high magnification.

Table 1. Grain morphology and hardness of as-fabricated NFA-1 specimens

Planes	Long, l (µm)	Short, s (µm)	Avg, d= l+s)/2 (µm)	Aspect ratio, r = l/s	Microhardness, HV, (Kg/mm^2)
LT (Face)	0.767 ± 0.566	0.517 ± 0.355	0.642 ± 0.450	1.5 ± 0.4	376 ± 18
LS (Front)	0.792 ± 0.638	0.301 ± 0.108	0.546 ± 0.343	2.7 ± 1.6	368 ± 25
TS (Side)	0.799 ± 0.833	0.296 ± 0.180	0.548 ± 0.482	2.7 ± 1.3	352 ± 39

Despite having uniformly distributed Y-Ti-O rich nano-oxides (NOs) (size: 2.1 nm, number density: 1.6 x 10^{23} m^{-3} and volume fraction: 0.25%) all over the NFA-1 matrix, reported elsewhere [2], the material also reveals the presence of relatively coarser precipitates (Figures 2b and 3b) in the matrix, summarized in Table 2. These precipitates are predominantly located at or near the grain boundaries in the form of stringers (Figure 3b). EDS equipped with SEM and TEM, identify them mostly as Ti-rich (darker) with some as Y-rich (relatively gray) oxides [5]. These stringers are oriented randomly at the plates' face but parallel to the extrusion or cross-rolling direction at the front and side views, respectively, with an average

stringer separation distance 2.6 to 2.8 µm (Table 2 and point 1 of Figure 3b). Average precipitate size is ≈ 60 nm, ranging from 10 to 262 nm. Figure 3c shows the distribution of coarser precipitate size. Table 2 also summarizes the spacing among the precipitates that averaged ~ 200 to 300 nm.

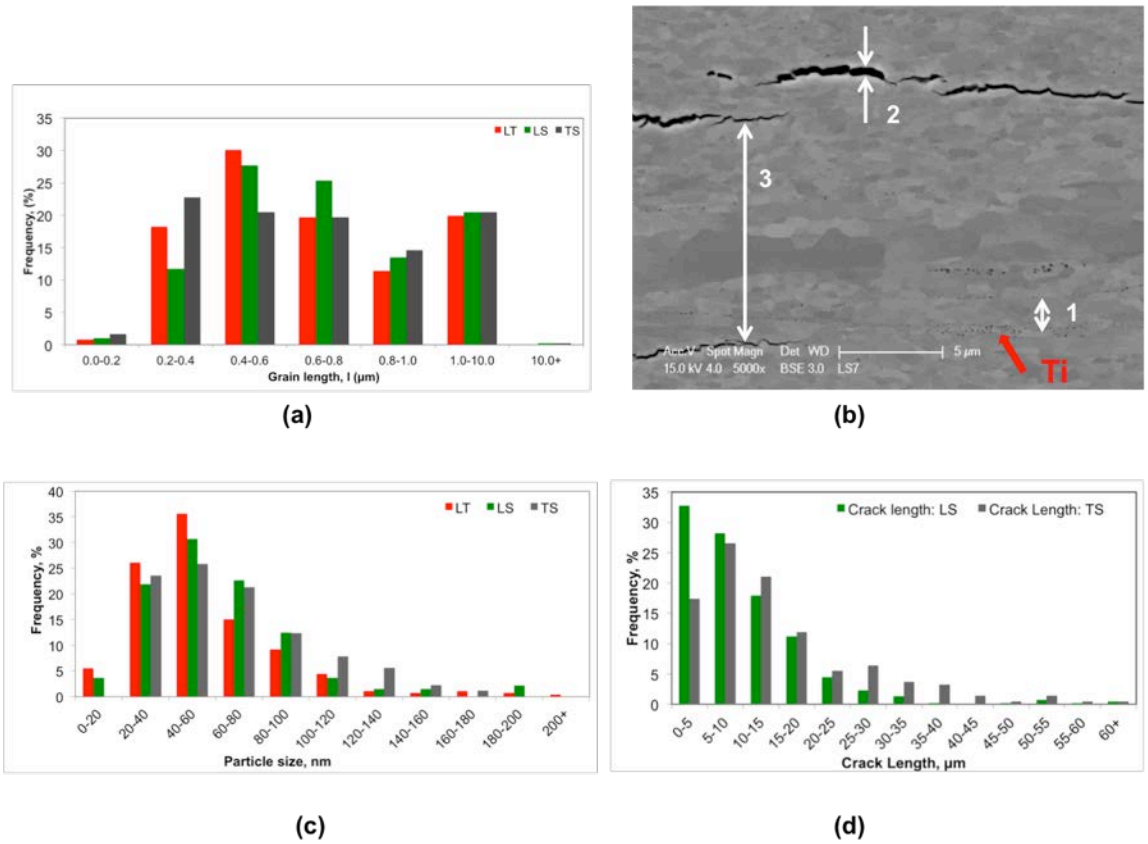

Figure 3. (a) Distribution of grain's length, l, (b) point 1, 2 and 3 showing the inter-stringer spacing, crack width and crack separation distance, respectively, (c) coarser particle size distribution, and (d) crack length distribution of as-fabricated NFA-1 plate at different plane views.

Table 2. Ti/Y rich precipitates of as-fabricated NFA-1

Planes	Ti/Y rich particle size (nm)	Interparticle spacing along x (nm)	String spacing along thickness (µm)
LT (Face)	57 ± 33	228 ± 106	Random
LS (Front)	62 ± 32	303 ± 210	2.6 ± 1.0
TS (Side)	68 ± 33	279 ± 160	2.8 ± 1.0

Figure 2 also shows the presence of microcracks running normal to the plate thickness direction both for the front (LS) and side (TS) plate views and their statistics are summarized in Table 3. The micro-mechanism of these crack formation has been reported elsewhere [5]. The average crack width (point 2 in Figure 3b), which is believed to be the initiation of crack front, is ~250 nm. The crack separation distance is measured between the layers of crack in the short thickness direction (point 3 in Figure 3b) and found almost same (~16 µm) for both the front and side views. Length of the cracks is also recorded and averaged ~10 µm (front) to 15 µm (side) with a span ranges from 2 µm to 105 µm. Smaller cracks might join together to form the larger cracks. In some cases, cracks are separated by a very small ligament (<1 µm) and might have minimal resistance during loading, and thus considered as a single large crack. Figure 3d shows almost similar crack size distribution for both front and side planes and

found ~75% cracks are below 15 µm with very few over 50 µm. Nevertheless, these larger cracks are supposed to serve as weaker links during fracture. The number density of cracks is also measured and found to be 2.5 times higher at the front than the side plane.

Table 3. Side surface crack statistics of as-fabricated NFA-1

Planes	Crack opening width (nm)	Crack separation distance (µm)	Crack length (µm)	Crack density (m^{-2})
LS (Front)	252 ± 142	16.3 ± 4.7	10.2 ± 8.9	3.45×10^9
TS (Side)	205 ± 130	15.2 ± 4.8	14.9 ± 12.6	1.34×10^9

Since the front and side plate view shows almost similar microstructural features for as-fabricated conditions, only the plates' side view (TS) has been considered for annealing along with its face (LT) view. Figure 4 and Tables 4 and 5 show the grain morphology and statistics of the face and side planes after annealing at 1300°C for 1 and 5 hrs. Results show that the introduction of annealing (1300 ^{o}C/1hr) increases the grain size up to 10%, which further increases with time (5hrs) ≈ 25% when compared with the as-fabricated condition. Aspect ratio of the side plane reduces from 2.7 for the as-fabricated condition to 1.8 for annealed at 1300°C/5h condition (Table 5). Grains larger than 10 µm were also not observed for any annealed specimen. Higher annealing temperature might recrystallize the larger grains. High temperature annealing also appears to heal the cracks, presumably by surface diffusion, perhaps assisted by recrystallization and grain boundary migration [6]. However, crater-like pores were observed in all the annealed specimens, and the size of these pores increases while their number decreases with annealing time.

Table 4. Grain morphology and hardness of NFA-1 as a function of annealing condition and plate views

Planes*	Long, l (µm)	Short, s (µm)	Avg, d= l+s)/2 (µm)	Aspect ratio	Microhardness, HV, (Kg/mm^2)
LTa131	0.842 ± 0.493	0.547 ± 0.285	0.695 ± 0.367	1.6 ± 0.4	294 ± 13
TSa131	0.849 ± 0.544	0.354 ± 0.144	0.602 ± 0.320	2.4 ± 1.3	304 ± 17
LTa135	0.979 ± 0.481	0.694 ± 0.325	0.837 ± 0.390	1.4 ± 0.4	252 ± 7
TSa135	0.963 ± 0.371	0.537 ± 0.197	0.750 ± 0.266	1.8 ± 0.5	247 ± 13

*LT: As-fabricated, LTa131: Annealed at **1300**^{o}C for **1** hr, LTa135: Annealed at **1300**^{o}C for **5** hrs

Microhardness

Vicker's microhardness (H_v) data for the as-fabricated and annealed NFA-1 are summarized in Tables 1 and 4, respectively. H_v averages 376 ± 18 (kg/mm^2) and 352 ± 39 (kg/mm^2) when indented at face and side plane, respectively. Hardness reduces ≈30% with the annealing for 1300°C/5hr. These differences can probably be attributed to the presence of pores and grain coarsening. However, unlike as-fabricated condition, hardness variation among different planes is negligible for annealed specimen.

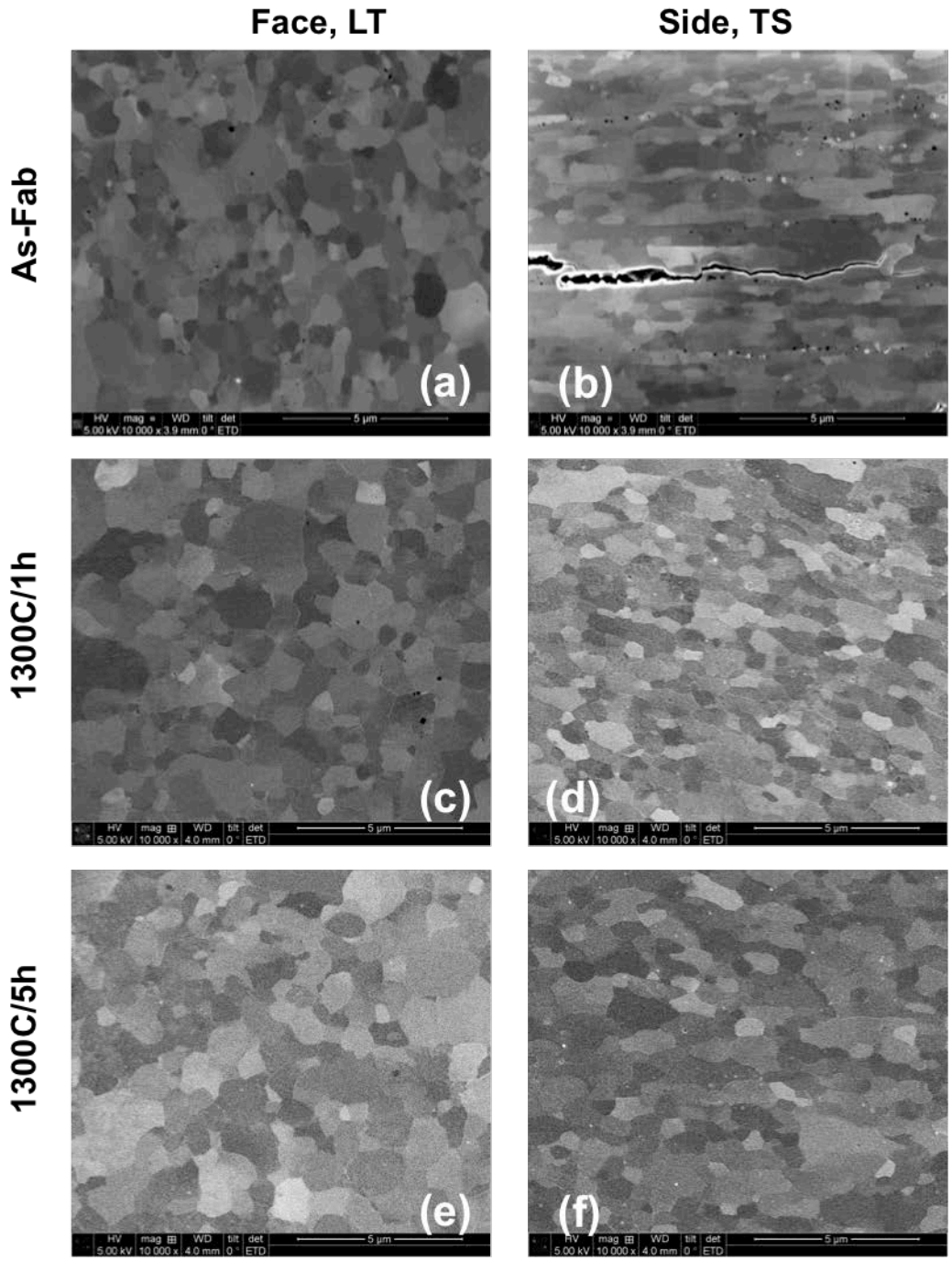

Figure 4. SEM/FIB images of the as-fabricated (a,b) and annealed (c-f) NFA-1 specimens for face (left column), and side (right column) planes, respectively.

Table 5. Grain aspect ratio, number and area fraction as a function of plates view, for as-fabricated and annealed conditions

Planes	Range (μm)	Length, l (μm)	Aspect ratio, r	No. freq. of grains, (%)	Area fraction, (%)
LT (Face)	0-1	0.57 ± 0.20	1.5 ± 0.4	80	60
	1-10	1.57 ± 0.80	1.6 ± 0.4	20	40
	10+	-	-	-	-
LS (Front)	0-1	0.60 ± 0.19	2.2 ± 0.7	79.3	64.6
	1-10	1.42 ± 0.50	4.5 ± 2.0	20.5	33.2
	10+	11.3	15.8	0.2	2.2
TS (Side)	0-1	0.56 ± 0.22	2.2 ± 0.9	79.3	59.5
	1-10	1.59 ± 0.94	4.1 ± 1.5	20.5	37.9
	10+	12.94	10.0	0.2	2.6
LT131 (face)	0-1	0.63 ± 0.19	1.5 ± 0.4	72.6	56
	1-10	1.40 ± 0.60	1.8 ± 0.6	27.4	44
	10+	-	-	-	-
TS131 (side)	0-1	0.60 ± 0.20	2.0 ± 0.7	72.8	55.2
	1-10	1.51 ± 0.61	3.5 ± 1.7	27.2	44.8
	10+	-	-	-	-
LT135 (Face)	0-1	0.71 ± 0.19	1.4 ± 0.4	61.1	45.2
	1-10	1.39 ± 0.50	1.5 ± 0.3	38.9	54.8
	10+	-	-	-	-
TS135 (Side)	0-1	0.72 ± 0.16	1.7 ± 0.4	59	45.6
	1-10	1.31 ± 0.29	2.0 ± 0.5	41	54.4
	10+	-	-	-	-

Tensile Properties

Results of low temperature uniaxial tensile test on L oriented specimens are shown in Table 6 and their engineering stress-strain s(e) curves at Figure 5. Unlike most of the metallic materials, the NFA-1 material shows a concurrent increase in strengths and ductility (except at -196°C) at sub-zero temperatures. For example, ~32% higher yield strength (YS) and ~65% higher uniform elongation (UE) has been observed for -150°C when compared to room temperature test. This exceptional phenomenon can be attributed to the presence of microcracks that creates delamination during the test (see Figure 6a). These delaminations split the thickness of the tensile specimen and drive them towards plane stress conditions, and thus, suppress the effect of friction stress or Peierls force. Strengths continue to increase (1469 MPa YS and 1563 MPa UTS) at liquid nitrogen temperature, while both the uniform and total elongation decreases to 1.0% and 8.4%, respectively. Relatively lower ductility at -196 ^{o}C might be due to the activation of Peierls stress, which might take control over delamination, or it might only happen to this particular specimen. Low magnification fracture image for -196°C, shown in Figure 6a, shows a relatively shiny fracture surface. Nevertheless, higher magnification images of the fractured specimens tested at all

different temperatures reveals almost identical flake-like shallow dimples, attributed to ductile tearing (Figure 6b). It is worth noting that the NFA-1 material showed remarkably low ductile brittle transition temperature (≈ -185 ^{o}C), reported previously [3], which makes the NFA-1 material to achieve near record strength-toughness combination. In contrast, The S tensile specimen tested at room temperature fails in a complete brittle manner, mostly in its elastic zone, with almost 0% ductility. The fractured surface shows a very flat, shiny face with cleavage like brittle features (see Figures 6 and 7). Upon loading, the pre-existing micro cracks that run perpendicular to the loading direction propagate by brittle cleavage.

Table 6. Low temperature tensile test results of L oriented NFA-1 specimens

Temperature (^{o}C)	0.2%YS (MPa)	UTS (MPa)	UE (%)	TE (%)
20	970	1062	6.4	13.9
-50	1046 ± 64	1143 ± 37	9.2 ± 0.3	16.1 ± 0.4
-100	1123	1249	9.9	16.0
-150	1283	1380	10.6	16.6
-196	1469	1563	1.0	8.4

YS= Yield strength, UTS= ultimate tensile strength, UE = uniform elongation, TE= total elongation.

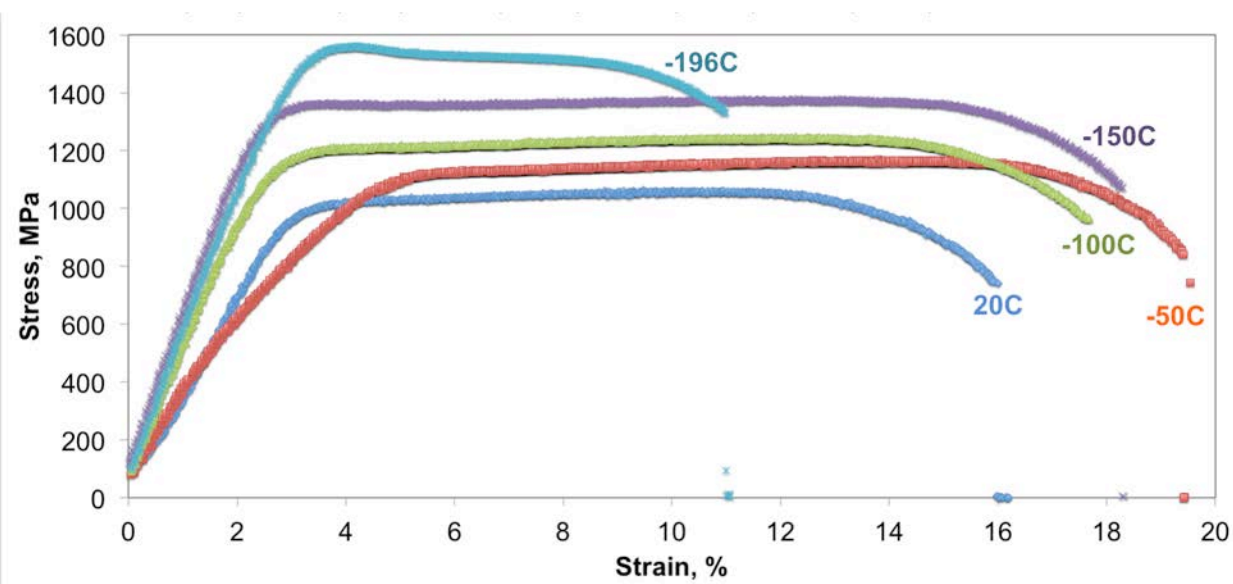

Figure 5. Engineering stress-strain curves of L-oriented NFA-1 specimens tested at lower temperatures.

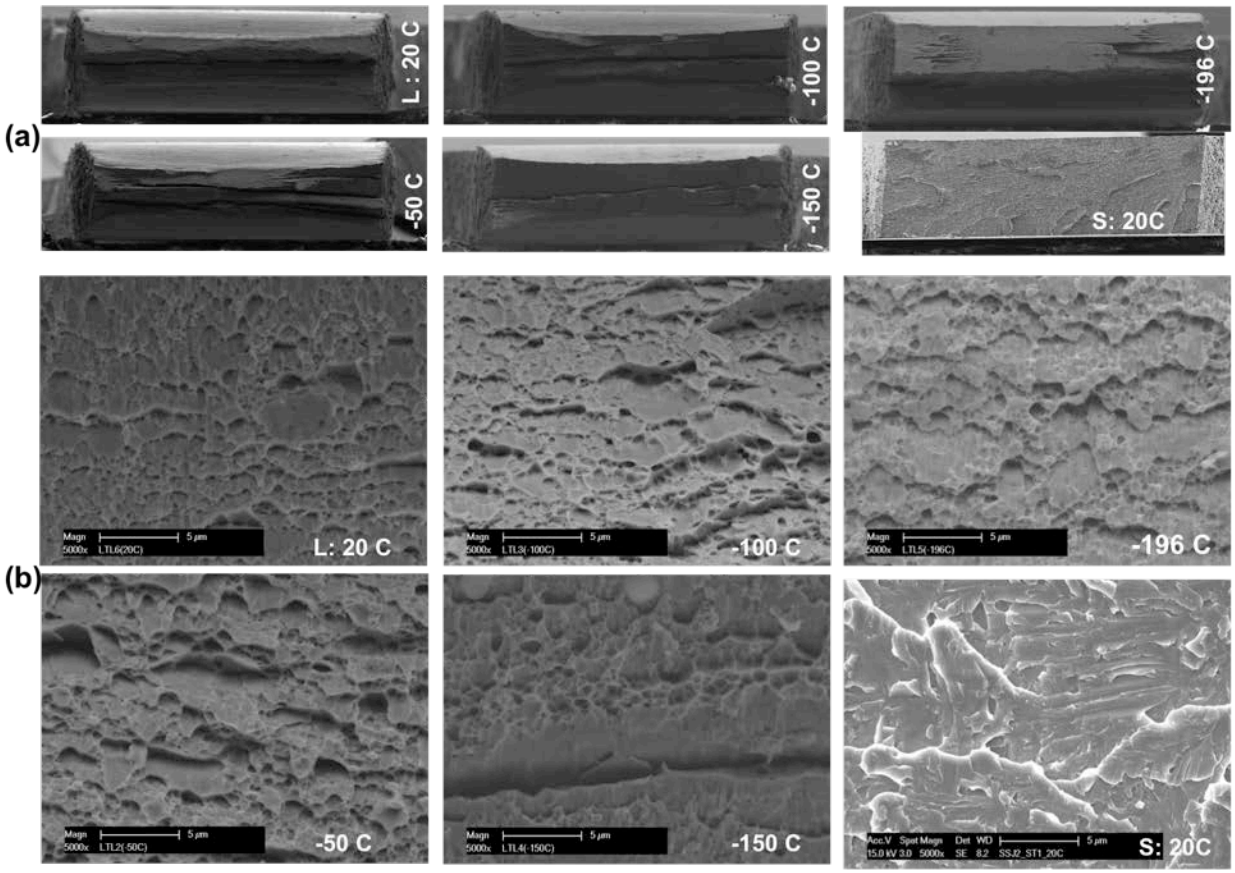

Figure 6. Low (a), and high (b) magnified SEM images of the L and S-oriented tensile fracture surfaces.

The room temperature tensile s(e) curves and their respective SEM fractographs of as-fabricated and annealed (with varying times) conditions for L and S oriented NFA-1 specimens are shown in Figure 7. Figure 8 also plots the summary of their properties. Annealing at 1300°C for 1 and 5 hrs lower the tensile strength for L by ~14% and ~24%, respectively, than their as-fabricated condition. Uniform and total elongation remain almost similar at all conditions though the fracture mechanism changes from delamination driven for as-fabricated specimens to microvoid coalescence dimple fracture with some presence of crater-like features for annealed specimens. These craters might be partly responsible for lower strength along with higher grain size compared to the as-fabricated specimens. While the as-fabricated S oriented tensile specimen failed in the elastic region at room temperature, the corresponding 1h annealed specimen has a large total elongation of ≈ 18% with a significantly higher UTS of ≈ 874 MPa compared to the as-fabricated condition (≈ 652 MPa). Annealing at 1300°C for 5h further improves the total ductility to 23%, while tensile strength drops slightly (≈ 802 MPa), but still high enough when compared with the as-fabricated condition. Fracture surface has also been changed from flat, shiny brittle fracture for as-fabricated specimens to dimple dominated ductile fracture with some craters for annealed specimens. The crater-like features may partially heal microcracks and help to increase the ductility. The room temperature strength and ductility of the L and S oriented annealed specimens are comparable to each other. These improvements in strength and ductility are associated with the absence of microcracks and grains larger than 10 µm (see Table 5 and Figure 4).

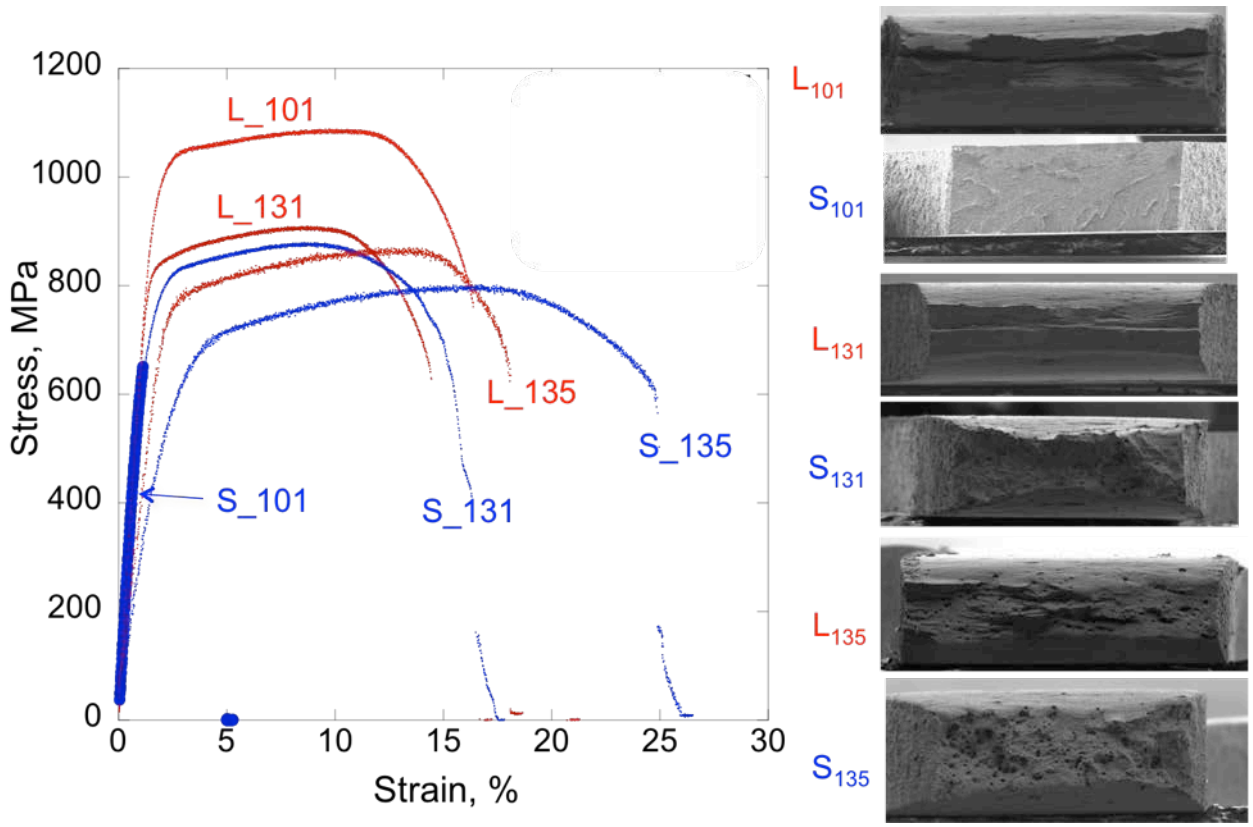

Figure 7. Room temperature engineering stress-strain curves for the as-fabricated and annealed L (red) and S (blue) oriented tensile specimens and their respective SEM fractographs. Codes 101, 131 and 135 mean as-fab, annealed at 1300°C/1hr and annealed at 1300°C/5hr conditions, respectively.

Fracture toughness

Room temperature fracture toughness test were conducted on L-T oriented as-fabricated and annealed (1300°C/1hr) specimens and their load-displacement curves along with fracture surfaces are shown in Figure 9. The results show that the toughness reduces ≈ 22% for the annealed specimen when compared with the as-fabricated specimen. This lower toughness for annealed specimen might be associated with the relatively higher grain size, lower strength, and formation of crater-like pores and absence of microcracks in favourable orientations. Fracture mode has also been changed from delamination driven for the as-fabricated specimens to the classical dimple fracture by micro void coalescence for annealed specimen.

SUMMARY

The statistical analysis of microstructural features of as-fabricated and annealed NFA-1 material has been studied. High temperature annealing at 1300°C for 1 and 5 hrs appears to heal the microcracks and alters the pancake-shaped grains towards more equiaxed than exist in the as-fabricated plate. Annealing for 1 and 5 hrs also increases the average grain size by ≈ 10% and ≈ 24%, reducing the microhardness by ≈ 18% and ≈ 30%, respectively. The room temperature L loaded tensile strengths also lower by up to 24%. Interestingly, the strength increases up to ≈ 34% for the S loaded annealed tensile specimens. Total ductility was also observed ≈23% for the annealed condition, when compared to the as-fabricated condition that showed ≈0% ductility. The room temperature tensile properties are more isotropic after annealing.

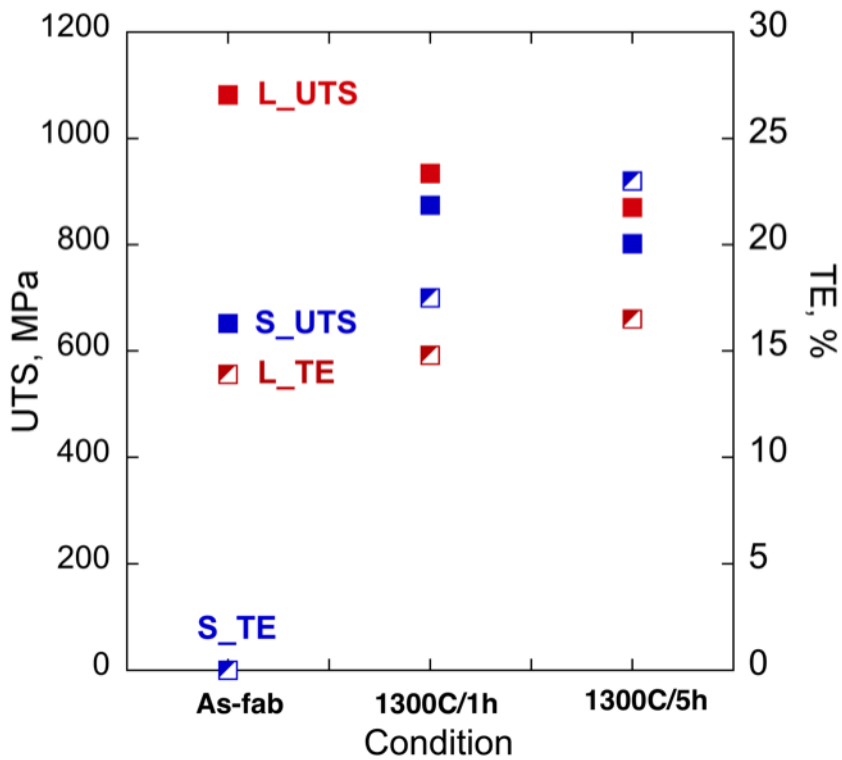

Figure 8. Room temperature ultimate tensile strength (UTS) and total elongation (TE) of L (red) and S (blue) oriented tensile specimens as a function of annealing conditions.

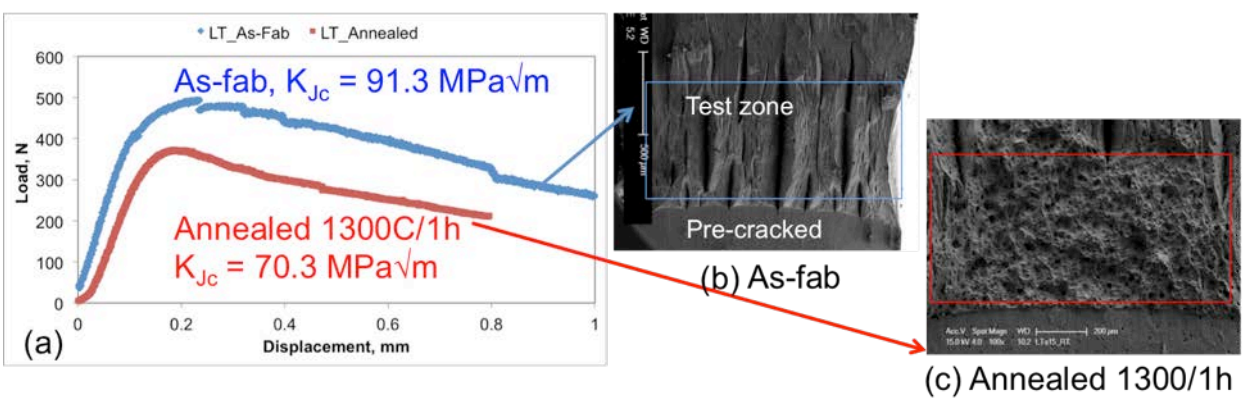

Figure 9. Room temperature fracture toughness test for L-T oriented specimens: (a) load-displacement curves, (b) delamination driven fracture for the as-fabricated specimen, and (c) dimple fracture surface for annealed at1300^{o}C/1hr specimens.

The effect of different annealing temperatures (1100 and 1200 ^{o}C) and times (1 and 5 hrs) will be explored and more detailed observations on microcrack healing will be obtained along with the corresponding effects on the grains, dislocations and NO nanostructures.

Acknowledgments

This work is part of a multi-laboratory collaboration between LANL, UCSB, and ORNL. The DOE Office of Fusion Energy Sciences supported some of the mechanical testing reported here. NFA-1 was produced under the sponsorship of the DOE Office of Nuclear Energy through a NEUP grant and the FCRD program.

References

[1] G.R. Odette, "Recent progress in developing and qualifying nanostructured ferritic alloys for advanced fission and fusion applications," JOM. 66 (2014) 2427.

[2] N.J. Cunningham, Y. Wu, G.R. Odette, D.T. Hoelzer, S.A. Maloy, " Characterization of a larger best practice heat of 14YWT in annealed powder, HIP consolidated and extruded forms", Fusion Materials Semiannual Progress Report for Period Ending June 30, 2013, DOE/ER-0313/54, U. S. Department of Energy, 15.

[3] M.E. Alam, NJ Cunningham, D. Gragg, K. Fields, G. R. Odette, D. T. Hoelzer and S. A. Maloy, "Mechanical Properties Characterization of a Larger Best Practice Heat of 14YWT NFA1", Fusion Materials Semiannual Progress Report for Period Ending June 30, 2014, DOE/ER-0313/56, U. S. Department of Energy.

[4] M.E. Alam, K. Fields, G. R. Odette, D. T. Hoelzer and S. A. Maloy, "Tensile property characterization of 14YWT nanostructured ferritic alloy NFA1" Fusion Materials Semiannual Progress Report for Period Ending December 31, 2014, DOE/ER-0313/57, U. S. Department of Energy, 39.

[5] S. Pal, M. E. Alam, G. R. Odette, D. Hoelzer and S. Maloy, " Microstructure, texturing, microcracking and delamination behavior of NFA-1", DOE/ER-0313/58 (2015), DOE Fusion Reactor Materials Program Semiannual Progress Report, 58 (2015) 66-82.

[6] K.W. Gao, L.J. Qiao, and W. Y. Chu, "In situ TEM observation of crack healing in □α-Fe", Scripta Materialia, 44 (2001) 1055.